ISSN 1674-1056
http://cpb.iphy.ac.cn
http://iopscience.iop.org/cpb
中国物理 B
Chinese Physics
中国物理 Chinese Physics B

Mechanism from particle compaction to fluidization of liquid-solid two-phase flow

Yue Zhang(张悦)[1], Jinchun Song(宋锦春)[1], Lianxi Ma(马连喜)[2], Liancun Zheng(郑连存)[3], Minghe Liu(刘明贺)[4]
Citation: Chin. Phys. B . 2020, 29(1): 014702 . **doi:** 10.1088/1674-1056/ab5789
Journal homepage: http://cpb.iphy.ac.cn; http://iopscience.iop.org/cpb

What follows is a list of articles you may be interested in

Studies of flow field characteristics during the impact of a gaseous jet on liquid-water column

Jian Wang(王健), Wen-Jun Ruan(阮文俊), Hao Wang(王浩), Li-Li Zhang(张莉莉)
Chin. Phys. B . 2019, 28(6): 064704 . **doi:** 10.1088/1674-1056/28/6/064704

Numerical simulations of dense granular flow in a two-dimensional channel:The role of exit position

Tingwei Wang(王廷伟), Xin Li(李鑫), Qianqian Wu(武倩倩), Tengfei Jiao(矫滕菲), Xingyi Liu(刘行易), Min Sun(孙敏), Fenglan Hu(胡凤兰), Decai Huang(黄德财)
Chin. Phys. B . 2018, 27(12): 124704 . **doi:** 10.1088/1674-1056/27/12/124704

Gradient-augmented hybrid interface capturing method for incompressible two-phase flow

Zheng Fu(付峥), Shi-Yu Wu(吴士玉), Kai-Xin Liu(刘凯欣)
Chin. Phys. B . 2016, 25(6): 064701 . **doi:** 10.1088/1674-1056/25/6/064701

Three-dimensional multi-relaxation-time lattice Boltzmann front-tracking method for two-phase flow

Hai-Qiong Xie(谢海琼), Zhong Zeng(曾忠), Liang-Qi Zhang(张良奇)
Chin. Phys. B . 2016, 25(1): 014702 . **doi:** 10.1088/1674-1056/25/1/014702

Multi-relaxation-time lattice Boltzmann front tracking method for two-phase flow with surface tension

Xie Hai-Qiong, Zeng Zhong, Zhang Liang-Qi, Liang Gong-You, Hiroshi Mizuseki, Yoshiyuki Kawazoe
Chin. Phys. B . 2012, 21(12): 124703 . **doi:** 10.1088/1674-1056/21/12/124703

Mechanism from particle compaction to fluidization of liquid–solid two-phase flow*

Yue Zhang(张悦)[1,†], Jinchun Song(宋锦春)[1], Lianxi Ma(马连喜)[2], Liancun Zheng(郑连存)[3], and Minghe Liu(刘明贺)[4]

[1] School of Mechanical Engineering and Automation, Northeastern University, Shenyang 110819, China
[2] Department of Physics, Blinn College, Bryan, TX77805, USA
[3] School of Mathematics and Physics of University of Science and Technology Beijing, Beijing 100083, China
[4] School of Mechanical Engineering, Shenyang Jianzhu University, Shenyang 110168, China

(Received 27 May 2019; revised manuscript received 22 September 2019; accepted manuscript online 14 November 2019)

A new model of particle yield stress including cohesive strength is proposed, which considers the friction and cohesive strength between particles. A calculation method for the fluidization process of liquid–solid two-phase flow in compact packing state is given, and the simulation and experimental studies of fluidization process are carried out by taking the sand–water two-phase flow in the jet dredging system as an example, and the calculation method is verified.

Keywords: liquid–solid flow, two-phase flow, cohesive strength, yield stress

PACS: 47.57.Gc, 47.61.Jd **DOI:** 10.1088/1674-1056/ab5789

1. Introduction

The process from compaction to fluidization of particles is common in dredging, fluidized bed, and mixing process. The study of this fluidization process can be used to optimize the structure and operating conditions of related equipments.[1–3]

In liquid and solid two-phase flow, the evolution process of particle phase from compaction to fluidization includes three stages: quasi-static flow, dense flow, and dilute flow.[4] Because of the different behaviors of particle phase in different stages,[5,6] the calculation methods of the three stages are different.

In the dilute flow stage, particles are fully fluidized and interact by binary collision. Sinclair *et al.*[7] used the kinetic theory of granular flow (KTGF) which considered collision as the main interaction between particles to study the flow properties and the calculation method of full developed gas and solid two-phase flow in a vertical tube. Upadhyay *et al.*[8] studied the gas–solid two-phase flow properties in a lab scale circulating fluidized bed riser based on KTGF. Wu *et al.*[9] applied KTGF to study the flow properties of dilute particles in vertical and inclined vessels. Mehran *et al.*[10] applied KTGF to study the flow properties and heat transfer behavior in a liquid–solid regenerative fluidized bed heat exchanger.

In the stage of dense flow, the particle phase is not fully fluidized, and the interactions between particles include binary collision and friction. Sofiane *et al.*[11] used KTGF combining frictional stress model which considered the collision and friction between particles to study the flow properties of dense gas and solid two-phase flow in a bin discharge. Ng *et al.*[12] used KTGF combining frictional stress model to study the kinetic and frictional contributions to granular motion in an annular Couette flow. Maryam *et al.*[13] studied dense gas–solid flow properties in a bubbling fluidized bed by applying KTGF combining frictional stress model. Wang *et al.*[14] studied the flow behavior of gas and particles in spouted beds by using KTGF combining frictional stress model. Srujal *et al.*[15,16] applied KTGF combining frictional stress model to study the dense gas and solid two-phase flow properties in a large-scale circulating fluidized bed. Abbas *et al.*[17] used KTGF combining frictional stress model to study liquid and solid two-phase flow properties in a circulating fluidized bed riser. Wang *et al.*[18] studied the hydrodynamic characteristics of particles in a liquid–solid fluidized bed by applying KTGF combining frictional stress model. Li *et al.*[19] used KTGF combining frictional stress model to study the behavior of solid and liquid two-phase flow in cross fractures.

In the stage of quasi-static flow, particles are packing closely, and the interactions between particles are different from those between particles in the stages of dense flow and dilute flow. Passalacqu *et al.*[20] used KTGF combining frictional stress model which considered the factors of friction and collision to study the behaviors of dry particles in a gas–solid bubbling fluidized bed from quasi-static flow to dilute flow. However, in the liquid and solid two-phase flow, the particles are wet, and the interactions between particles in the quasi-static flow stage are different from those of dry particles.

In a spraying dredging system, sediment particles are fluidized by jet flow. The particles are fluidized from quasi-static

*Project supported by the National Natural Science Foundation of China (Grant No. 11772046) and the Young Scientists Fund of the National Natural Science Foundation of China (Grant No. 51705342).

†Corresponding author. E-mail: zhangyue12342280@sina.com

© 2020 Chinese Physical Society and IOP Publishing Ltd

flow to dilute flow in the whole fluidization process. In prior analysis of the process, the authors used KTGF combining frictional stress model which only considered the factors of collision and friction to study the behaviors of the particles. But the computed results did not agree well with the experimental data. Therefore, in this paper, the interactions of collision, friction, and cohesive strength between particles are considered to study the flow properties of liquid and solid two-phase flow in the fluidization process. A particle yield stress model including cohesive strength is established, and a calculation method for such process is presented.

2. Methodology

2.1. Continuity equations

The two-fluid model is used to describe the liquid–solid two phases. The mass and momentum equations are written as follows:

$$\frac{\partial}{\partial t}(\alpha_{\mathrm{L}}\rho_{\mathrm{L}})+\nabla\cdot(\alpha_{\mathrm{L}}\rho_{\mathrm{L}}v_{\mathrm{L}})=0, \tag{1}$$

$$\begin{aligned}&\frac{\partial}{\partial t}(\alpha_{\mathrm{L}}\rho_{\mathrm{L}}v_{\mathrm{L}})+\nabla\cdot(\alpha_{\mathrm{L}}\rho_{\mathrm{L}}v_{\mathrm{L}}v_{\mathrm{L}})\\ &=-\alpha_{\mathrm{L}}\nabla p_{\mathrm{L}}+\nabla\tau_{\mathrm{L}}+\alpha_{\mathrm{L}}\rho_{\mathrm{L}}g-\beta(v_{\mathrm{L}}-v_{\mathrm{S}}),\end{aligned} \tag{2}$$

$$\frac{\partial}{\partial t}(\alpha_{\mathrm{S}}\rho_{\mathrm{S}})+\nabla\cdot(\alpha_{\mathrm{S}}\rho_{\mathrm{S}}v_{\mathrm{S}})=0, \tag{3}$$

$$\begin{aligned}&\frac{\partial}{\partial t}(\alpha_{\mathrm{S}}\rho_{\mathrm{S}}v_{\mathrm{S}})+\nabla\cdot(\alpha_{\mathrm{S}}\rho_{\mathrm{S}}v_{\mathrm{S}}v_{\mathrm{S}})\\ &=-\alpha_{\mathrm{S}}\nabla p_{\mathrm{L}}+\nabla\tau_{\mathrm{S}}+\alpha_{\mathrm{S}}\rho_{\mathrm{S}}g+\beta(v_{\mathrm{L}}-v_{\mathrm{S}}).\end{aligned} \tag{4}$$

In the above equations, the subscripts L and S denote the liquid and particles, respectively, ρ is the density, v is the velocity, p is the pressure, α is the volume fraction of liquid and particles, and β is the drag coefficient. The drag coefficient β is defined as[21]

$$\beta=\begin{cases}150\dfrac{\alpha_{\mathrm{S}}(1-\alpha_{\mathrm{L}})\mu_{\mathrm{L}}}{\alpha_{\mathrm{L}}d_{\mathrm{S}}^2}+1.75\dfrac{\rho_{\mathrm{L}}\alpha_{\mathrm{S}}|v_{\mathrm{S}}-v_{\mathrm{L}}|}{d_{\mathrm{S}}}, & \alpha_{\mathrm{S}}\geqslant 0.2,\\ \dfrac{3}{4}C_{\mathrm{D}}\dfrac{\alpha_{\mathrm{S}}\alpha_{\mathrm{L}}\rho_{\mathrm{L}}|v_{\mathrm{S}}-v_{\mathrm{L}}|}{d_{\mathrm{S}}}\alpha_{\mathrm{L}}^{-2.65}, & \alpha_{\mathrm{S}}<0.2.\end{cases} \tag{5}$$

The drag coefficient for single particle C_{D} and Reynolds number of particle phase Re_{S} are defined as

$$C_{\mathrm{D}}=\frac{24}{\alpha_{\mathrm{L}}Re_{\mathrm{S}}}\left[1+0.15(\alpha_{\mathrm{L}}Re_{\mathrm{S}})^{0.687}\right], \tag{6}$$

$$Re_{\mathrm{S}}=\frac{\alpha_{\mathrm{L}}\rho_{\mathrm{L}}d_{\mathrm{S}}|v_{\mathrm{L}}-v_{\mathrm{S}}|}{\mu_{\mathrm{L}}}. \tag{7}$$

2.2. Stress of granular phase

Because of the different behaviors of granular flow in different concentrations, the shear stress of granular phase is divided into two regimes of dilute flow and dense flow

$$\tau_{\mathrm{S}}=\begin{cases}\tau_{\mathrm{S,dil}}, & \alpha_{\mathrm{S}}<\alpha_{\mathrm{S,min}},\\ \tau_{\mathrm{S,des}}, & \alpha_{\mathrm{S}}\geqslant\alpha_{\mathrm{S,min}},\end{cases} \tag{8}$$

where $\alpha_{\mathrm{S,min}}$ is the critical frictional volume fraction of particles, $\alpha_{\mathrm{S,min}}=0.5$.

In the dilute flow regime, the particle stress is written as

$$\tau_{\mathrm{S,dil}}=(-p_{\mathrm{S}}+\lambda_{\mathrm{S}}\nabla\cdot v_{\mathrm{S}})I+2\mu_{\mathrm{S}}S_{\mathrm{S}}, \tag{9}$$

where p_{S} is the particle pressure, λ_{S} is the bulk viscosity of the particle phase, μ_{S} is the shear viscosity of the particle phase, and S_{S} is the strain rate of the particle phase expressed as

$$S_{\mathrm{S}}=\frac{1}{2}(\nabla v_{\mathrm{S}}+\nabla v_{\mathrm{S}}^{\mathrm{T}})-\frac{1}{3}\nabla\cdot v_{\mathrm{S}}I. \tag{10}$$

According to the kinetic theory of granular flows,[21–27] the particle pressure is composed of motion and collision terms[23]

$$p_{\mathrm{S}}=p_{\mathrm{SC}}=\alpha_{\mathrm{S}}\rho_{\mathrm{S}}\Theta_{\mathrm{S}}+2\rho_{\mathrm{S}}(1+e_{\mathrm{SS}})\alpha_{\mathrm{S}}^2g_{0,\mathrm{SS}}\Theta_{\mathrm{S}}, \tag{11}$$

where p_{SC} is the particle pressure composed of motion and collision terms; e_{SS} is the collision recovery coefficient, $0<e_{\mathrm{SS}}<1$; $g_{0,\mathrm{SS}}$ is the radial distribution function; and Θ_{S} is the particle temperature.

Bulk viscosity λ_{S} is written as[26]

$$\lambda_{\mathrm{S}}=\frac{4}{3}\alpha_{\mathrm{S}}\rho_{\mathrm{S}}d_{\mathrm{S}}g_{0,\mathrm{SS}}(1+e_{\mathrm{SS}})(\Theta_{\mathrm{S}}/\pi)^{1/2}. \tag{12}$$

The μ_{S} is composed of dynamic viscosity $\mu_{\mathrm{S,kin}}$ and collision viscosity $\mu_{\mathrm{S,col}}$,[23]

$$\mu_{\mathrm{S}}=\mu_{\mathrm{S,col}}+\mu_{\mathrm{S,kin}}, \tag{13}$$

$$\mu_{\mathrm{S,col}}=\frac{4}{5}\alpha_{\mathrm{S}}\rho_{\mathrm{S}}d_{\mathrm{S}}g_{0,\mathrm{SS}}(1+e_{\mathrm{SS}})(\Theta_{\mathrm{S}}/\pi)^{1/2}\alpha_{\mathrm{S}}, \tag{14}$$

$$\mu_{\mathrm{S,kin}}=\frac{10d_{\mathrm{S}}\sqrt{\Theta_{\mathrm{S}}\pi}}{96\alpha_{\mathrm{S}}(1+e_{\mathrm{SS}})g_{0,\mathrm{SS}}}\left[1+\frac{4}{5}g_{0,\mathrm{SS}}\alpha_{\mathrm{S}}(1+e_{\mathrm{SS}})\right]^2\alpha_{\mathrm{S}}. \tag{15}$$

Radial distribution function $g_{0,\mathrm{SS}}$ is defined as[23]

$$g_{0,\mathrm{SS}}=\left[1-(\alpha_{\mathrm{S}}/\alpha_{\mathrm{S,max}})^{1/3}\right]^{-1}. \tag{16}$$

Particle temperature Θ_{S} denotes the intensity of particle movement, $\Theta_{\mathrm{S}}=\frac{1}{3}\overline{v_{\mathrm{S}}'v_{\mathrm{S}}'}$. The transport equation of Θ_{S} is given by[27]

$$\begin{aligned}&\frac{3}{2}\left[\frac{\partial}{\partial t}(\alpha_{\mathrm{S}}\rho_{\mathrm{S}}\Theta_{\mathrm{S}})+\nabla\cdot(\alpha_{\mathrm{S}}\rho_{\mathrm{S}}v_{\mathrm{S}}\Theta_{\mathrm{S}})\right]\\ &=(-p_{\mathrm{S}}I+\tau_{\mathrm{S}}):\nabla v_{\mathrm{S}}+\nabla\cdot(k\nabla\Theta_{\mathrm{S}})-\gamma+3\beta\Theta_{\mathrm{S}},\end{aligned} \tag{17}$$

$$\begin{aligned}k=&\frac{150\rho_{\mathrm{S}}d_{\mathrm{S}}\sqrt{\Theta_{\mathrm{S}}\pi}}{384(1+e_{\mathrm{SS}})g_{0,\mathrm{SS}}}\left[1+\frac{6}{5}\alpha_{\mathrm{S}}g_{0,\mathrm{SS}}(1+e_{\mathrm{SS}})\right]^2\\ &+2\rho_{\mathrm{S}}\alpha_{\mathrm{S}}^2d_{\mathrm{S}}g_{0,\mathrm{SS}}(1+e_{\mathrm{SS}})\sqrt{\Theta_{\mathrm{S}}/\pi},\end{aligned} \tag{18}$$

$$\gamma=\frac{12(1-e_{\mathrm{SS}}^2)g_{0,\mathrm{SS}}}{d_{\mathrm{S}}\sqrt{\pi}}\rho_{\mathrm{S}}\alpha_{\mathrm{S}}^2\Theta_{\mathrm{S}}^{3/2}. \tag{19}$$

In the dense flow regime, the particle stress is written as

$$\tau_{\mathrm{s,des}}=(-p_{\mathrm{S}}+\lambda_{\mathrm{S}}\nabla\cdot v_{\mathrm{s}})I+2\mu_{\mathrm{S}}S_{\mathrm{S}}+\tau_{\mathrm{y}}, \tag{20}$$

where τ_{y} is the yield stress of solid phase. Taking into account of the friction between particles, p_{S} is defined as[28]

$$p_{\mathrm{S}}=p_{\mathrm{SC}}+p_{\mathrm{fr}}, \tag{21}$$

$$p_{\mathrm{fr}}=0.05\frac{(\alpha_{\mathrm{S}}-\alpha_{\mathrm{S,min}})^2}{(\alpha_{\mathrm{S,max}}-\alpha_{\mathrm{S}})^5}. \tag{22}$$

2.3. Yield stress of granular phase

When the particles are packed in the liquid phase, the yield stress of granular phase should be composed of two parts: the friction and cohesive strength between the particles. So, the particle yield stress τ_y is defined as

$$\tau_y = (\tau_c + \tau_f) S_S / \|S_S\|, \tag{23}$$

where $\|S_S\| = \sqrt{\frac{1}{2} S_S : S_S}$, τ_f represents the frictional interaction between particles, and τ_c represents the cohesive strength between particles.

The frictional stress of the particle phase conforms to Coulomb's law

$$\tau_f = p_{fr} \sin\varphi, \tag{24}$$

where φ is the initial friction angle.

In this paper, we consider that the cohesive strength is related to the volume fraction of the particle phase. And when $\alpha_S < \alpha_{S,min}$, the cohesive strength does not exist between particles. According to Ref. [29], the cohesive strength is defined as

$$\tau_c = \begin{cases} \dfrac{n\alpha_{S,max}}{d_S}\left[2.5\left(\dfrac{\alpha_S}{\alpha_{S,max}}\right)^{1.5} + 120\left(\dfrac{\alpha_S}{\alpha_{S,max}}\right)^{6}\right], & \alpha_S \geqslant \alpha_{S,min}, \\ 0, & \alpha_S < \alpha_{S,min}, \end{cases} \tag{25}$$

where n is the coefficient of cohesive strength and its order of magnitude is 10^{-4} g/cm. When $n = 0$, it means that the cohesive strength is ignored.

3. Experiment and simulation

3.1. Experimental system

In order to study the influence of cohesive strength, an experimental jet dredging system is established, as shown in Fig. 1. Sand is packed at the bottom of the tank ④. Since the sand is immersed in water, cohesive strength exists between the wet sand particles. A jet flow sprays out from the injection tube ③, and fluidizes the sand. Then, the fluidized sand is sucked out from the suction pipe ⑤. In solid–liquid separator ⑦, sand and water are separated.

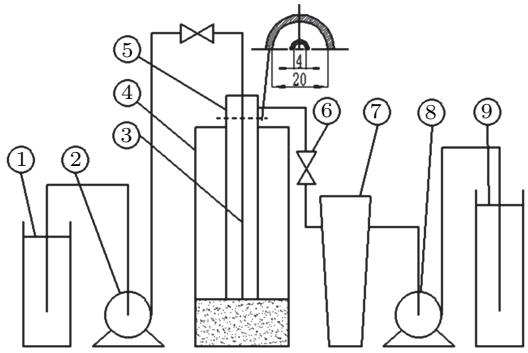


Fig. 1. Experimental system and the structure of calculation region: ① injection tank; ② injection pump; ③ injection tube; ④ tank; ⑤ suction tube; ⑥ valve; ⑦ separator; ⑧ suction pump; ⑨ suction tank.

3.2. Simulation method and boundary conditions

We apply the CFD solver Fluent to simulate the fluidization progress of sand and water in the jet dredging system. The structure of calculation region is shown in Fig. 2. In order to avoid the influence of air, the area within the red line is regarded as the calculation region. Because of the structural symmetry, an axial symmetry model is used to simplify the calculation. The calculation region is meshed in a structured grid. The minimum grid size is 1 mm. The jet pipe is the velocity inlet, the suction tube is the pressure outlet, and the upper boundary of water is the pressure inlet. The time step is 0.001 s, and the calculation time is 30 s. The averaged diameter of sand particles is 0.26 mm, the density of liquid phase is 983 kg/m^3, the liquid viscosity is 0.001 kg/ms, the solid density is 2550 kg/m^3, the maximum packing limit is 0.64, and the initial volume fraction of the particle phase is 0.6.

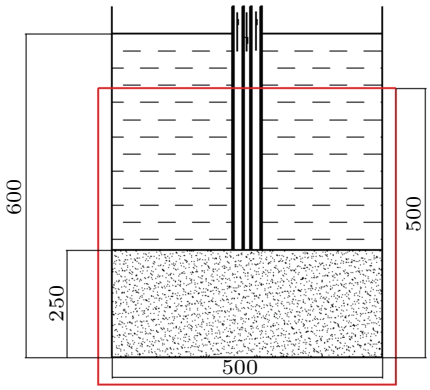


Fig. 2. The structure of calculation region.

3.3. Simulation results and discussion

In the process of sand collection, the fluidization region is formed by the impact of jet flow. The fluidization effect can be compared by the width and deepness of the fluidized region. In this paper, $\alpha_s = 0.55$ is taken as the critical volume fraction for the fluidization region. Figure 3 shows the boundary of the fluidized regions with different cohesive strength coefficients, where the jet flow rate $Q_i = 45$ g/s and the suction flow rate $Q_s = 50$ g/s. In Fig. 3, r_z is the distance from the center of the injection pipe to the boundary, h is the deepness of the fluidized region, and r is the radius of the suction pipe.

It can be found in Fig. 3 that, when $n = 0$, the maximum radii of fluidization area are greater than the experimental results. When n increases, the maximum radii of fluidized region decrease, and the depth of the fluidization area increases. When $n \geq 0.0002$ g/cm, the fluidization regions agree well with the experimental results.

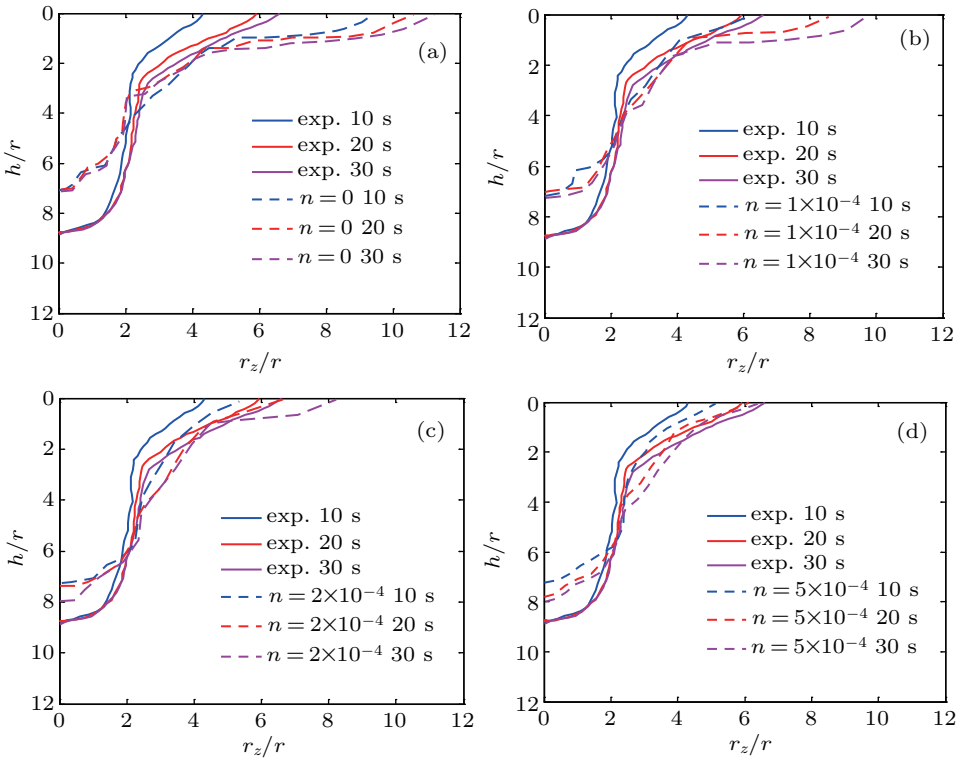


Fig. 3. Boundary of the fluidized regions with different cohesive strength coefficients: (a) $n = 0$, (b) $n = 0.0001$ g/cm, (c) $n = 0.0002$ g/cm, (d) $n = 0.0005$ g/cm.

The fluidization effect is also shown by the fluidized volume. Figure 4 shows the relation between the fluidized volume and collecting time ($Q_i = 45$ g/s, $Q_s = 50$ g/s). When $n = 0$, the fluidized volume of granular phase increases faster than the experimental results from 0 to 10 s. When n increases, the increasing rate of the fluidized volume decreases. When $n = 0.0002$ g/cm, the calculation results agree well with the experimental results.

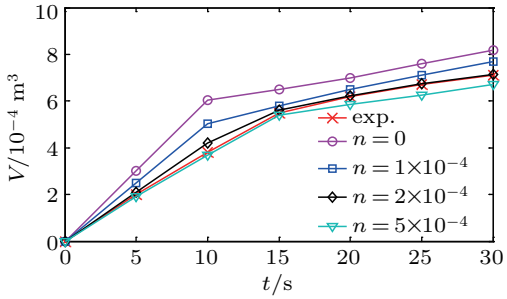


Fig. 4. The relation between fluidized volume and collecting time.

Figure 5 shows the relation between the averaged mass concentration of particle phase and rate of suction flow at the outlet ($Q_i = 45$ g/s). As shown in Fig. 5, the maximum averaged mass concentration is around 33% in experimental results. However, when $n = 0$, the maximum averaged mass concentration is around 45%. The averaged mass concentration decreases with the increasing cohesive strength coefficient. When $n = 0.0002$ g/cm, the averaged mass concentration of particle phase agrees well with the experimental results.

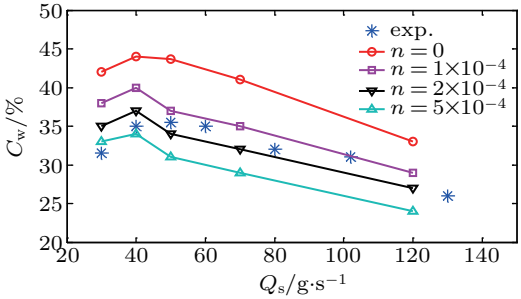


Fig. 5. Relation between averaged mass concentration of particle phase and rate of suction flow.

4. Conclusion

In summary, when $n = 0$, the yield stress of the granular phase is underestimated due to the neglect of the cohesive strength between particles in the sand–water two-phase flow. Taking the influence of the cohesive strength between particles into account, we have established a yield stress model of particle phase in this paper. A calculation method for fluidization process of liquid–solid two-phase flow in compact packing state is presented. Comparing with the simulation and experimental study, we find that when cohesive strength coeffi-

cient $n = 0.0002$ g/cm, the calculation results agree well with the experimental data.

References

[1] Hosseini S H, Zivdar M and Rahimi R 2009 *Che. Eng. Proce.* **48** 1539
[2] Seyyed H H, Goodarz A, Rahbar R, Mortaza Z and Mohsen N E 2010 *Powder Technol.* **200** 202
[3] Abbas D, Chao Z and Jingxu Z 2015 *Particuology* **21** 48
[4] Riccardo A, Alberto Z, Alessandra P, Paolo C and Andrea S 2011 *Che. Eng. Sci.* **66** 548
[5] Pierre J 2015 *C. R. Phys.* **16** 62
[6] Riccardo A, Andrea S and Paolo C 2009 *Che. Eng. Sci.* **64** 4040
[7] Sinclair J L and Jackson R 1989 *AIChE J.* **35** 1473
[8] Upadhyay M and Park J H 2015 *Powder Technol.* **272** 260
[9] Wu C L and Zhan J M 2005 *Chin. Phys. B* **14** 0620
[10] Mehran E, Salman M and Shahrokh S 2016 *Int. J. Therm. Sci.* **102** 111
[11] Sofiane B 2008 *Ind. Eng. Chem. Res.* **47** 8926
[12] Ng B H, Ding Y L and Ghadiri M 2008 *Che. Eng. Sci.* **63** 1733
[13] Maryam A, Mohammad S S, Hamid R G and Günter W 2015 *Powder Technol.* **274** 379
[14] Wang S Y, Li X, Lu H L a, Yu L, Sun D, He Y R and Ding Y L 2009 *Powder Technol.* **196** 184
[15] Srujal S, Kari M, Sirpa K and Timo H 2015 *Particuology* **18** 66
[16] Srujal S, Kari M, Sirpa K, Jouni R and Timo H 2015 *Powder Technol.* **274** 239
[17] Abbas D, Zhu J X and Zhang C 2014 *Powder Technol.* **260** 52
[18] Wang S Y, Zhao Y Q, Li X Q, Liu L L, Wei L X, Liu Y and Gao J S 2014 *Adv. Powder Technol.* **25** 1103
[19] Li P, Zhang X H and Lu X B 2018 *Che. Eng. Sci.* **181** 1
[20] Passalacqu A and Marmo L 2009 *Che. Eng. Sci.* **64** 2795
[21] Ding J and Gidaspow D 1990 *AICHE J.* **36** 523
[22] Chapman S and Cowling T G 1979 *The Mathematical Theory of Non-Uniform Gases* (London: Cambridge University Press)
[23] Gidaspow D 1994 Multiphase Flow and Fluidization Continuum and Kinetic Theory Descriptions (San Diego: Academic)
[24] Savage S B and Jeffrey D J 1981 *J. Fluid Mech.* **110** 255
[25] Jenkins J T and Savage S B 1983 *J. Fluid Mech.* **130** 187
[26] Lun C K K, Savage F B, Jeffrey D J and Chepurniy N 1984 *J. Fluid Mech.* **140** 223
[27] Syamlal M, Rogers W and O'Brien T J 1993 *MFIX Documentation: Volume 1 Theory Guide,* Technical Report DOE/METC-9411004 NTIS/DE9400087 (Springfield: National Technical Information Service)
[28] Johnson P C and Jackson R 1987 *J. Fluid Mech.* **176** 67
[29] Tang C B 1981 *J. Sediment Res.* **2** 60 (in Chinese)